Robust Diagnosis of Microstrip Planar Phased Arrays Through a Compressive Sensing Approach

M. Salucci, A. Gelmini, G. Oliveri, and A. Massa

Abstract

This work deals with the detection of faulty radiators in real microstrip patches planar phased arrays. Towards this goal, the diagnosis problem at hand is formulated within a probabilistic compressive sensing (*CS*) framework in order to avoid the fulfillment of the restricted isometry property (RIP) by the involved measurement operator. A customized Bayesian *CS* solution approach is then developed to yield robust and reliable guesses of the antenna under test (*AUT*) status by also taking into account all mutual coupling effects arising in realistic operative conditions. Some numerical benchmarks are shown to assess the effectiveness of the proposed diagnosis tool when considering a variation of the antenna size and failure rate, as well as a change of the amount of noise on processed far-field data.

Contents

1 Numerical Assessment

1.1 Microstrip Array, $N = 144$ Elements

Parameters

- Gold Array
  - Frequency: $f = 3.6$ $[GHz]$;
  - Number of elements along x and y: $N_x = N_y = 12$;
  - Total number of elements: $N = N_x \times N_y = 144$;
  - Spacing along x and y: $d_x = d_y = 0.5$ $[\lambda]$;
  - Excitation tapering: Slepian [1];
  - Angular region at the receiver: $\Psi = \{(u, v) : -u_0 \leq u \leq u_0, -v_0 \leq v \leq v_0\}$, with$u_0 = v_0 = 0.1$ [1];

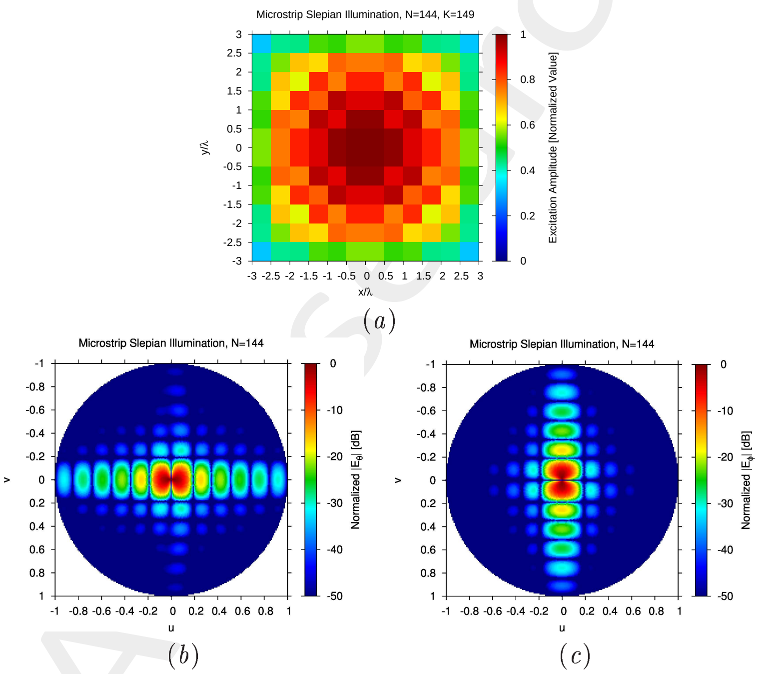

Figure 1: (a) Array excitations and normalized $(b)|E_\theta(u, v)|$ and $(c)|E_\phi(u, v)|$ patterns of the gold array.

- Failed Array
  - Failure factor: $\kappa = 0$ (total failures);
  - Failure rate: see table below;

N_f	$\Phi = \frac{N_f}{N}$
1	1%
3	2%
6	4%
12	8%
14	10%
17	12%
23	16%
29	20%

Table 1: Number of failures (N_f) and corresponding failure rate ($\Phi = \frac{N_f}{N}$).

- Measurement set-up
  - Type of sampling: uniform sampling in the (u, v) plane;
  - Number of points along u and v: $K_u = K_v = 15$;
  - Number of points in the visible range: $K = 149$;
  - Ratio between measurements and number of elements: $\nu = \frac{K}{N} \simeq 1.0$ $(\nu^{(opt)})$;
- BCS solver
  - Noise variance: $\eta = 5 \times 10^{-1}$ $(\eta^{(opt)})$;
  - Tolerance factor: $\iota = 10^{-8}$;
- Signal-to-Noise-Ratio: $SNR = \{10; 20; ...; 100\}$.

Results

$\Phi = \frac{N_f}{N} = 1\%$ ($N_f = 1$) - Best and Worst BCS Reconstructions

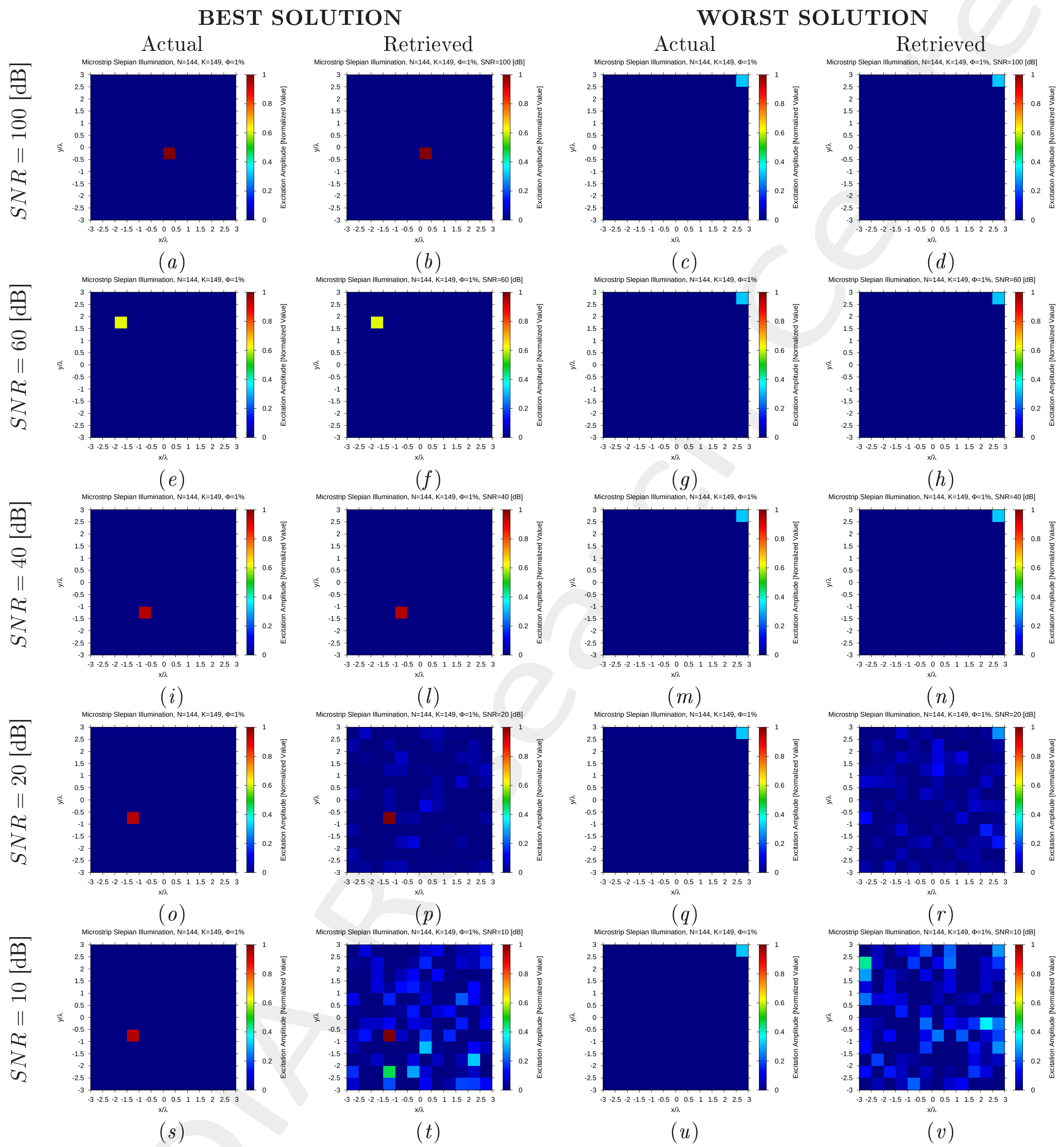

Figure 2: *Microstrip Patches Array* ($N = 144$, $d_x = d_y = 0.5$ [λ], $\Phi = 1\%$) - Best and worst reconstructions under several SNR values.

$\Phi = \frac{N_f}{N} = 2\%$ $(N_f = 3)$ - **Best and Worst** BCS **Reconstructions**

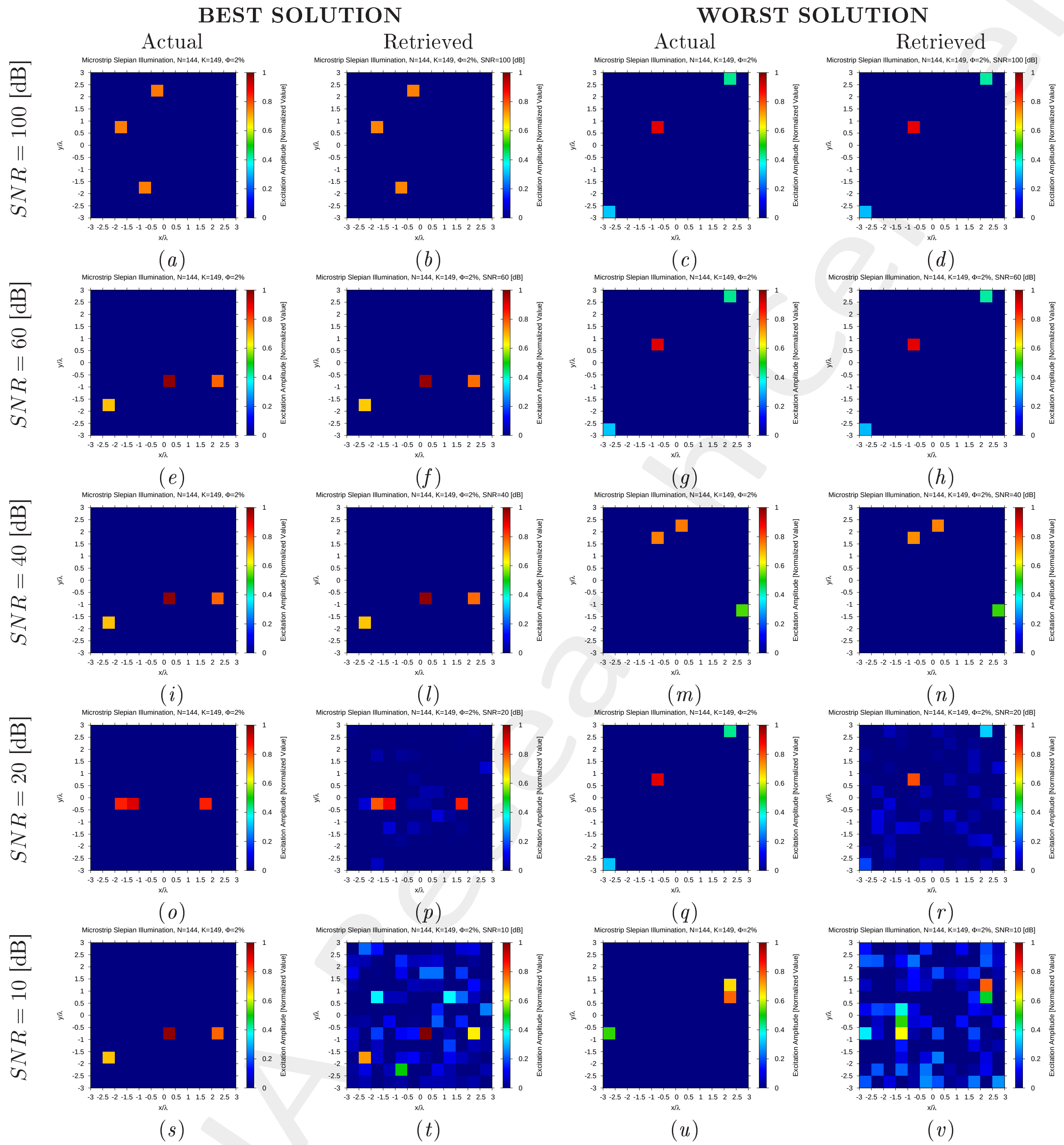

Figure 3: *Microstrip Patches Array* ($N = 144$, $d_x = d_y = 0.5$ [λ], $\Phi = 2\%$) - Best and worst reconstructions b under several SNR values.

$\Phi = \frac{N_f}{N} = 4\%$ ($N_f = 6$) - **Best and Worst** BCS **Reconstructions**

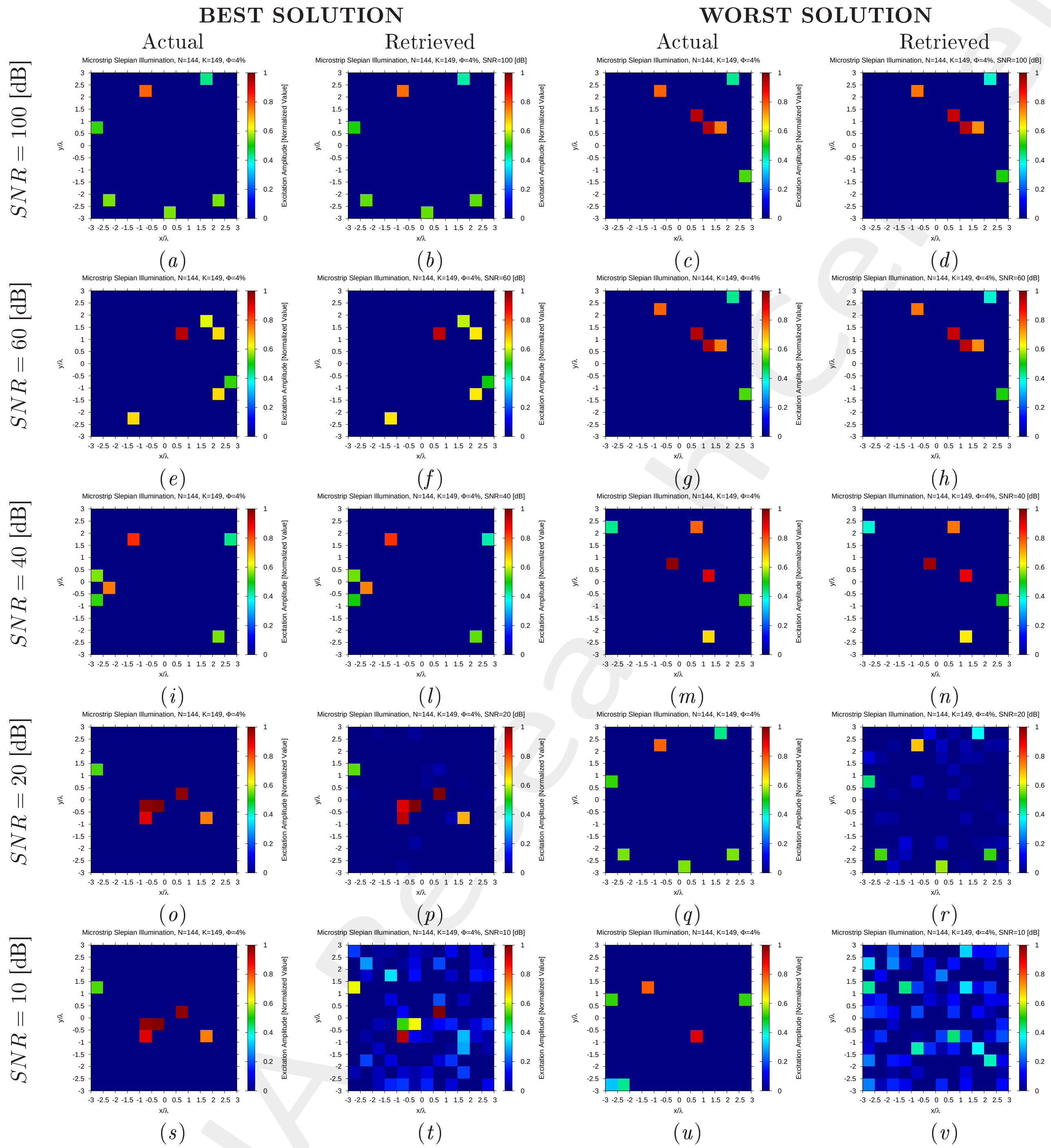

Figure 4: *Microstrip Patches Array* ($N = 144$, $d_x = d_y = 0.5$ [λ], $\Phi = 4\%$) - Best and worst reconstructions under several SNR values.

$\Phi = \frac{N_f}{N} = 8\%$ ($N_f = 12$) - **Best and Worst** ***BCS*** **Reconstructions**

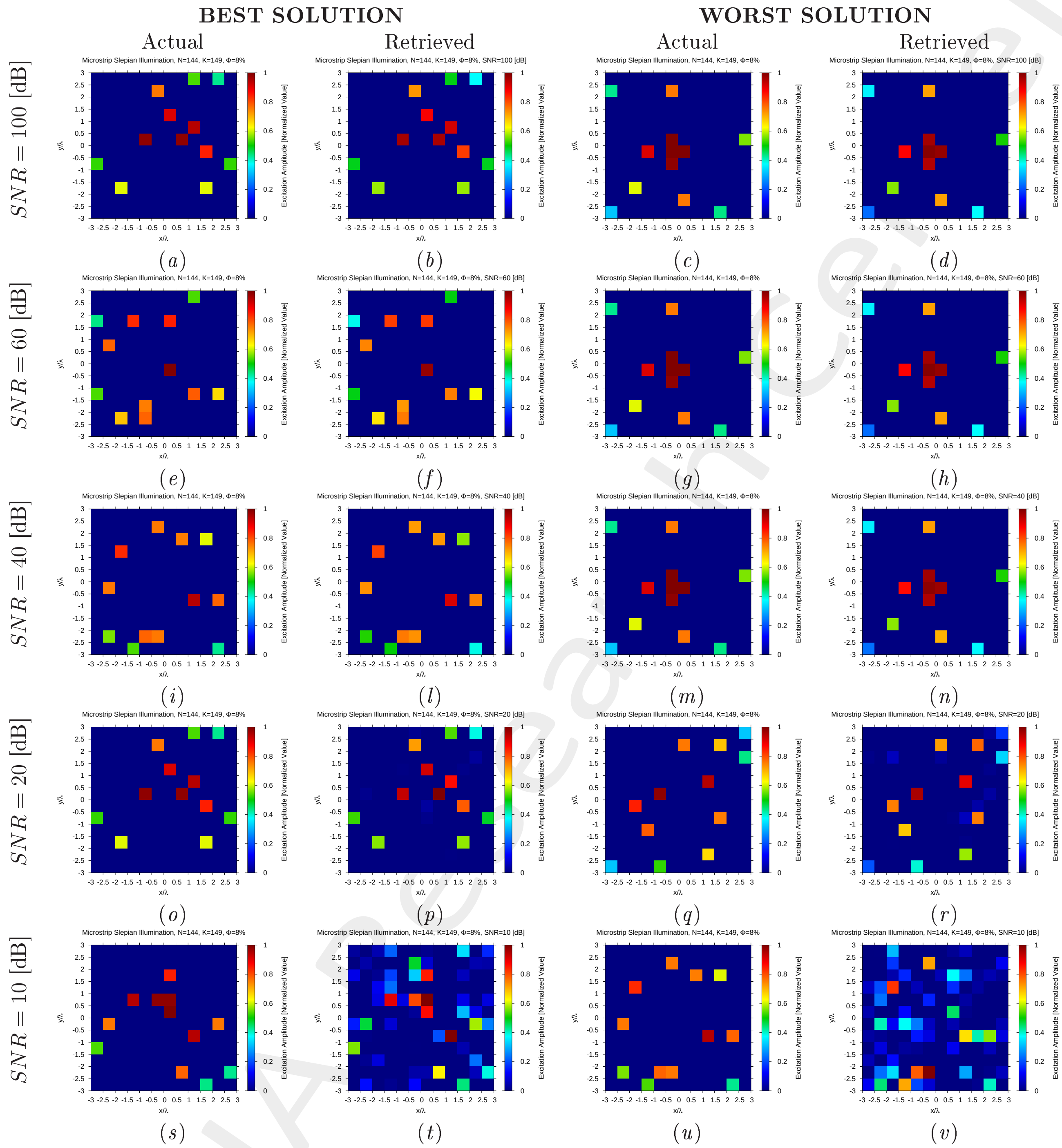

Figure 5: *Microstrip Patches Array* ($N = 144$, $d_x = d_y = 0.5$ [λ], $\Phi = 8\%$) - Best and worst reconstructions under several SNR values.

$\Phi = \frac{N_f}{N} = 16\%$ $(N_f = 23)$ - **Best and Worst** BCS **Reconstructions**

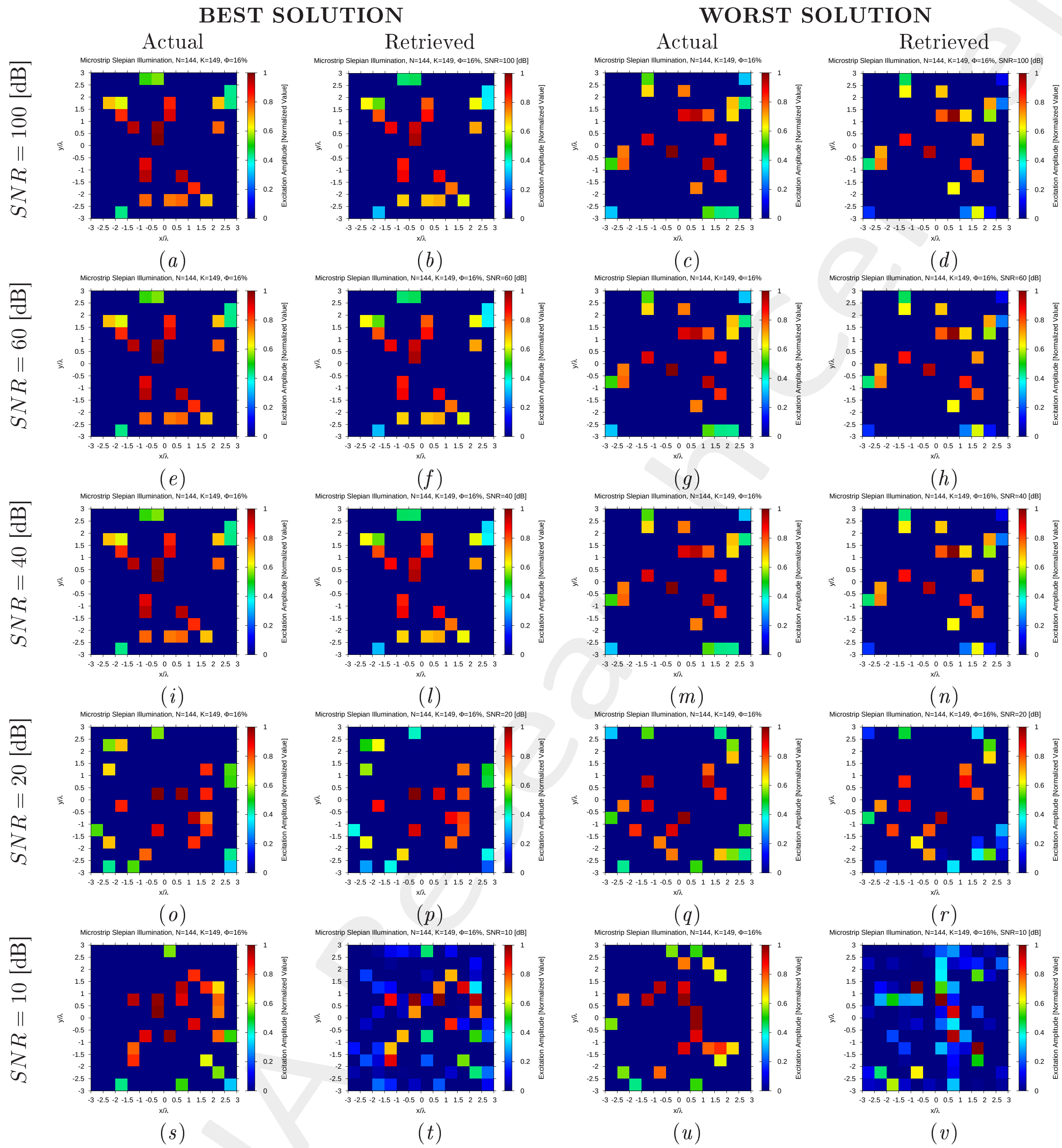

Figure 6: *Microstrip Patches Array* ($N = 144$, $d_x = d_y = 0.5$ [λ], $\Phi = 16\%$) - Best and worst reconstructions under several SNR values.

Diagnosis Error and Confidence Level

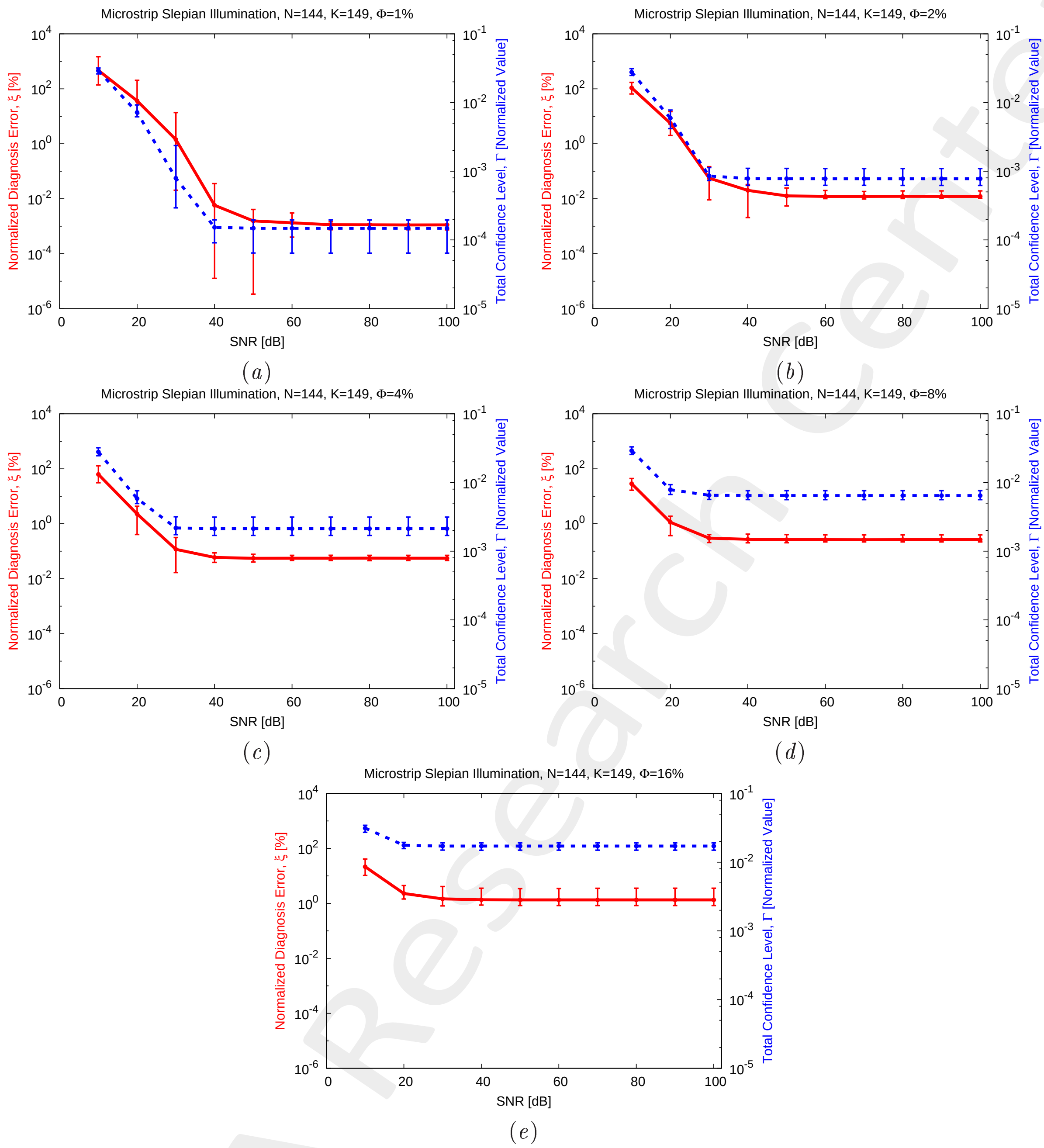

Figure 7: *Microstrip Patches Array* ($N = 144$, $d_x = d_y = 0.5$ $[\lambda]$) - Behavior of the average, minimum and maximum diagnosis error (ξ) and total confidence level (Γ) versus the SNR, for (a) $\Phi = 1\%$, (b) $\Phi = 2\%$, (c) $\Phi = 4\%$, (d) $\Phi = 8\%$, and (e) $\Phi = 16\%$.

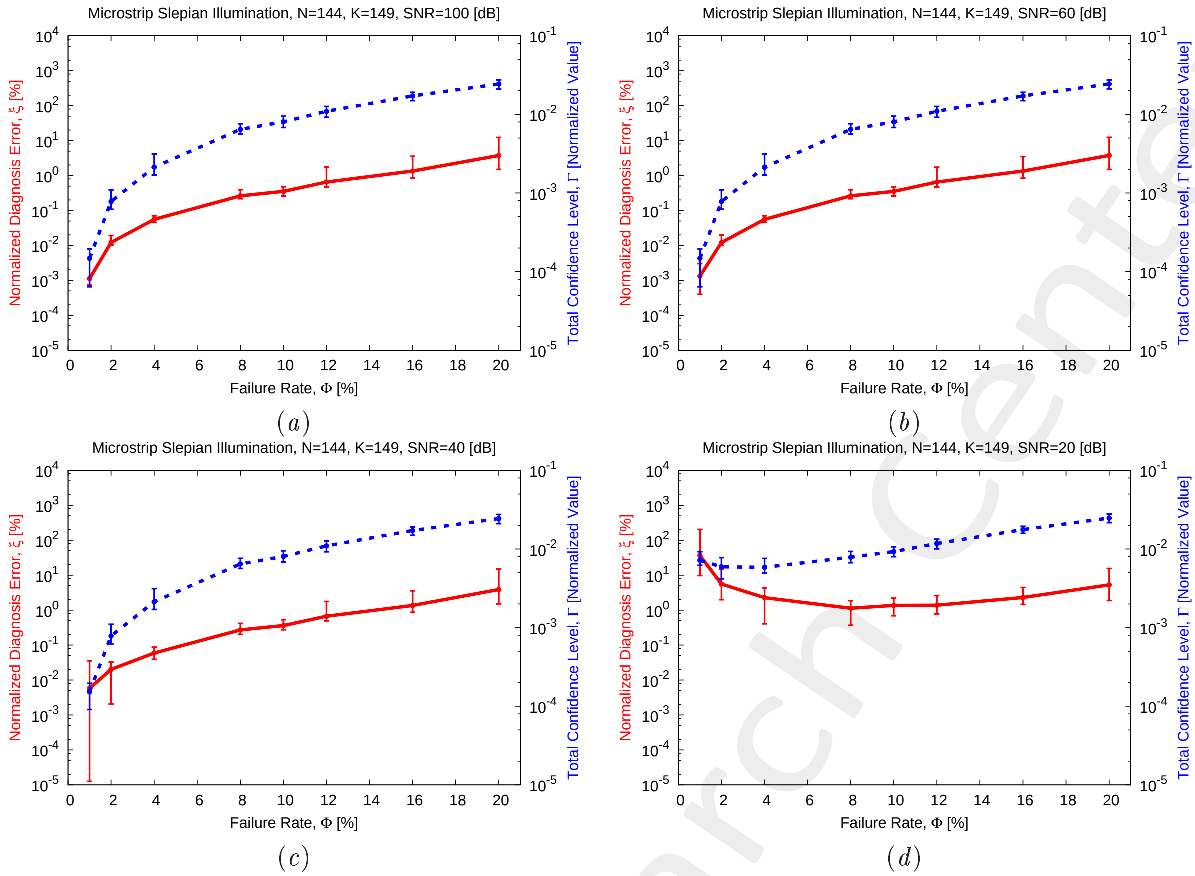

Figure 8: *Microstrip Patches Array* ($N = 144$, $d_x = d_y = 0.5$ [λ]) - Behavior of the average, minimum and maximum diagnosis error (ξ) and total confidence level (Γ) versus the failure rate (Φ), for (a) $SNR = 100$ [dB], (b) $SNR = 60$ [dB], (c) $SNR = 40$ [dB], and (d) $SNR = 20$ [dB].

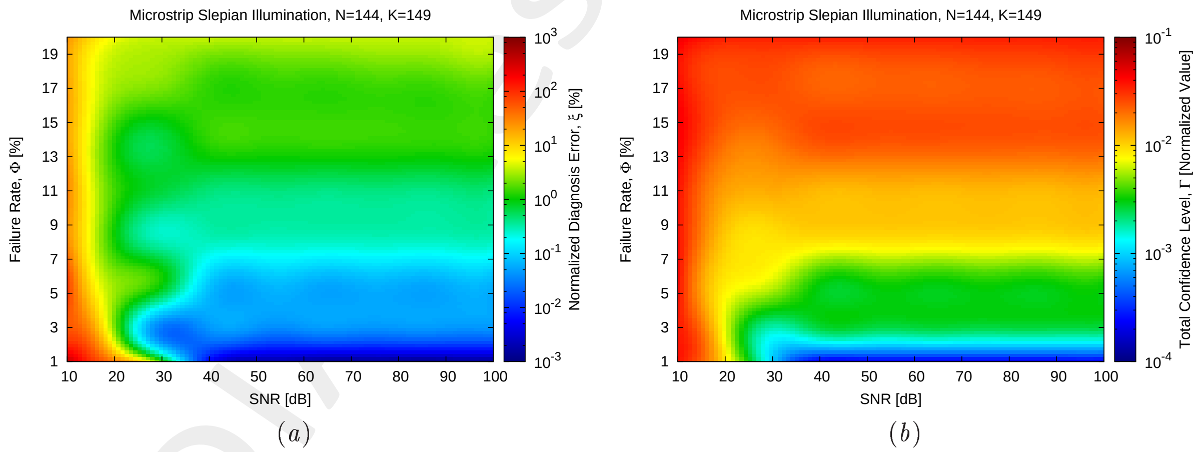

Figure 9: *Microstrip Patches Array* ($N = 144$, $d_x = d_y = 0.5$ [λ]) - Behavior of the average diagnosis error (ξ) and total confidence level (Γ) versus the SNR and the failure rate (Φ).

1.2 Microstrip Array, $N = 324$ Elements

Parameters

- Gold Array
  - Frequency: $f = 3.6$ $[GHz]$;
  - Number of elements along x and y: $N_x = N_y = 18$;
  - Total number of elements: $N = N_x \times N_y = 324$;
  - Spacing along x and y: $d_x = d_y = 0.5$ $[\lambda]$;
  - Excitation tapering: Slepian [1];
  - Angular region at the receiver: $\Psi = \{(u, v) : -u_0 \leq u \leq u_0, \ -v_0 \leq v \leq v_0\}$, with$u_0 = v_0 = 0.1$ [1];

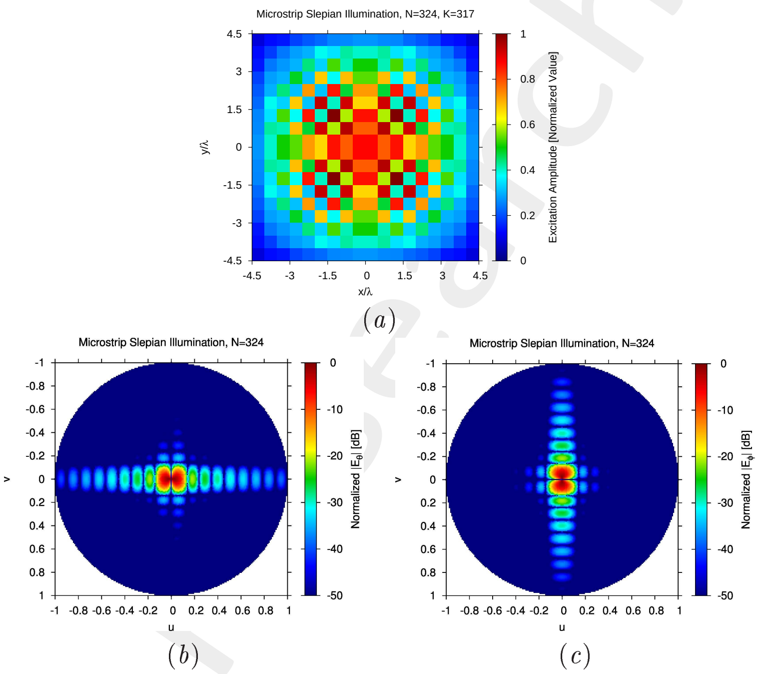

Figure 10: (a) Array excitations and normalized $(b)|E_\theta(u, v)|$ and $(c)|E_\phi(u, v)|$ patterns of the gold array.

- Failed Array
  - Failure factor: $\kappa = 0$ (total failures);
  - Failure rate: see table below;

N_f	$\Phi = \frac{N_f}{N}$
3	1%
6	2%
13	4%
26	8%
32	10%
39	12%
52	16%
65	20%

Table 2: Number of failures (N_f) and corresponding failure rate ($\Phi = \frac{N_f}{N}$).

- Measurement set-up
  - Type of sampling: uniform sampling in the (u, v) plane;
  - Number of points along u and v: $K_u = K_v = 21$;
  - Number of points in the visible range: $K = 317$;
  - Ratio between measurements and number of elements: $\nu = \frac{K}{N} \simeq 1.0$ ($\nu^{(opt)}$);
- BCS solver
  - Noise variance: $\eta = 5 \times 10^{-1}$ ($\eta^{(opt)}$);
  - Tolerance factor: $\iota = 10^{-8}$;
- Signal-to-Noise-Ratio: $SNR = \{10; 20; ...; 100\}$.

Results

$\Phi = \frac{N_f}{N} = 1\%$ $(N_f = 3)$ - Best and Worst BCS Reconstructions

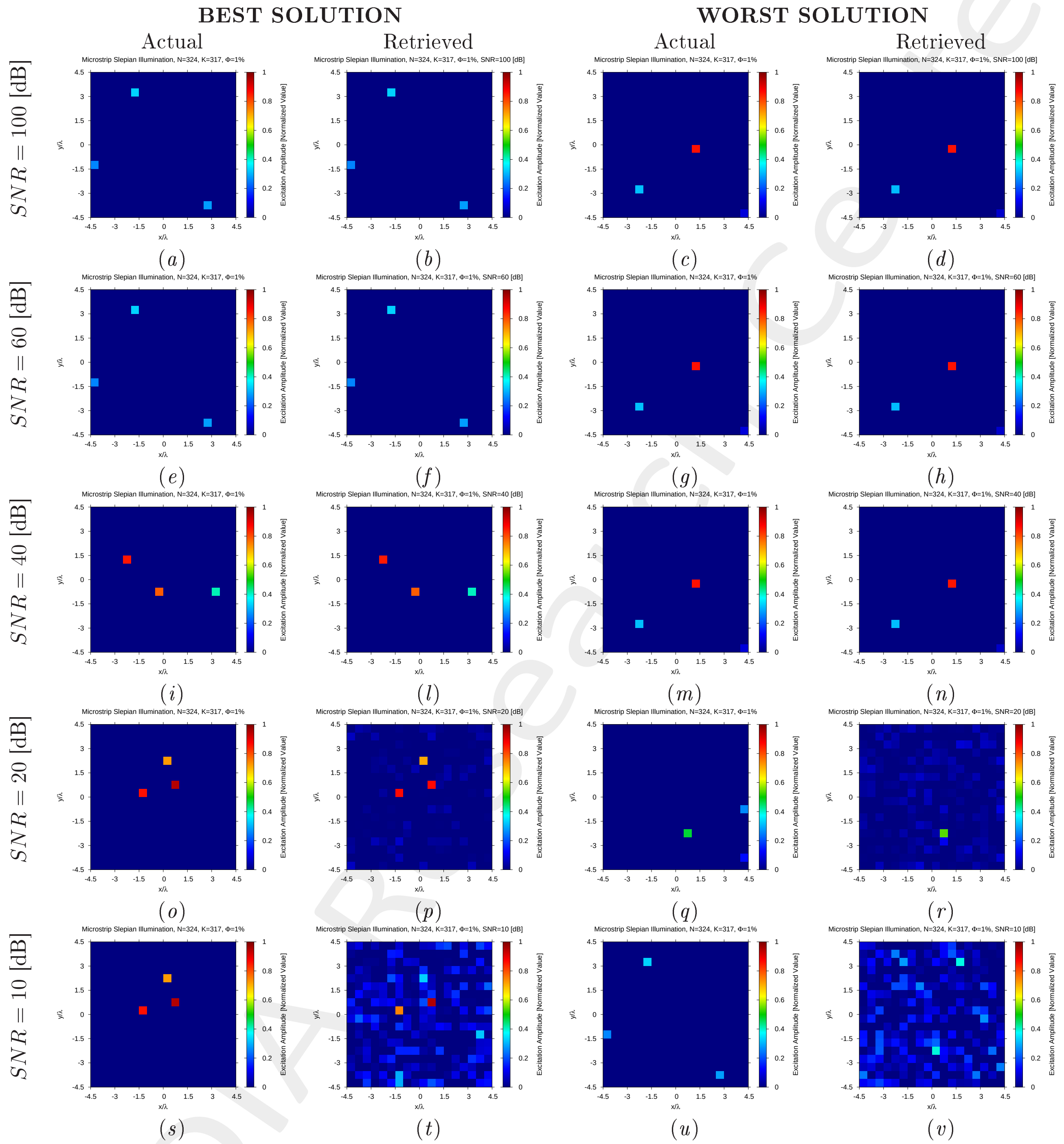

Figure 11: *Microstrip Patches Array* ($N = 324$, $d_x = d_y = 0.5$ [λ], $\Phi = 1\%$) - Best and worst reconstructions under several SNR values.

$\Phi = \frac{N_f}{N} = 2\%$ $(N_f = 6)$ - **Best and Worst** BCS **Reconstructions**

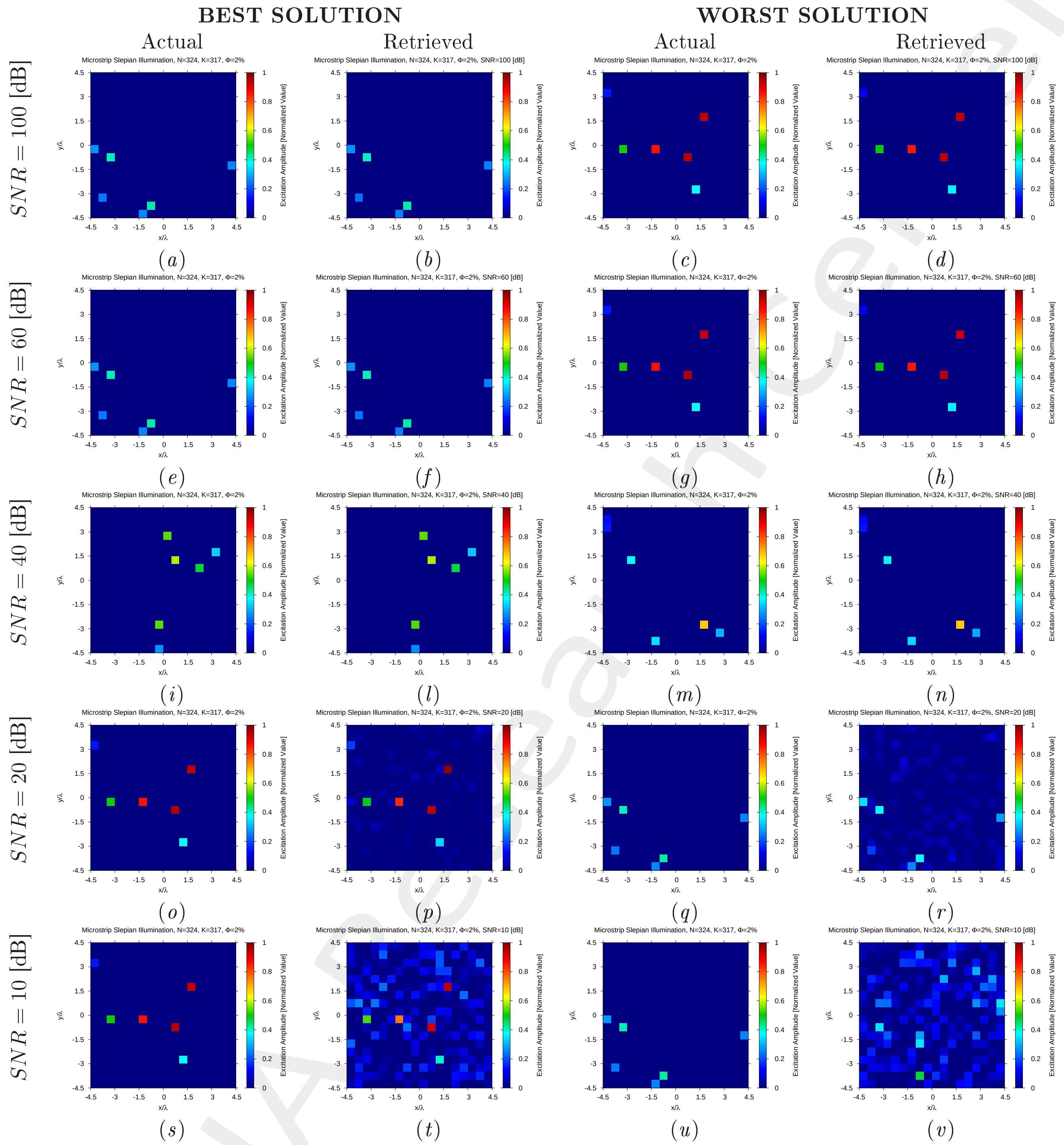

Figure 12: *Microstrip Patches Array* ($N = 324$, $d_x = d_y = 0.5$ $[\lambda]$, $\Phi = 2\%$) - Best and worst reconstructions under several SNR values.

$\Phi = \frac{N_f}{N} = 4\%$ $(N_f = 13)$ **- Best and Worst** BCS **Reconstructions**

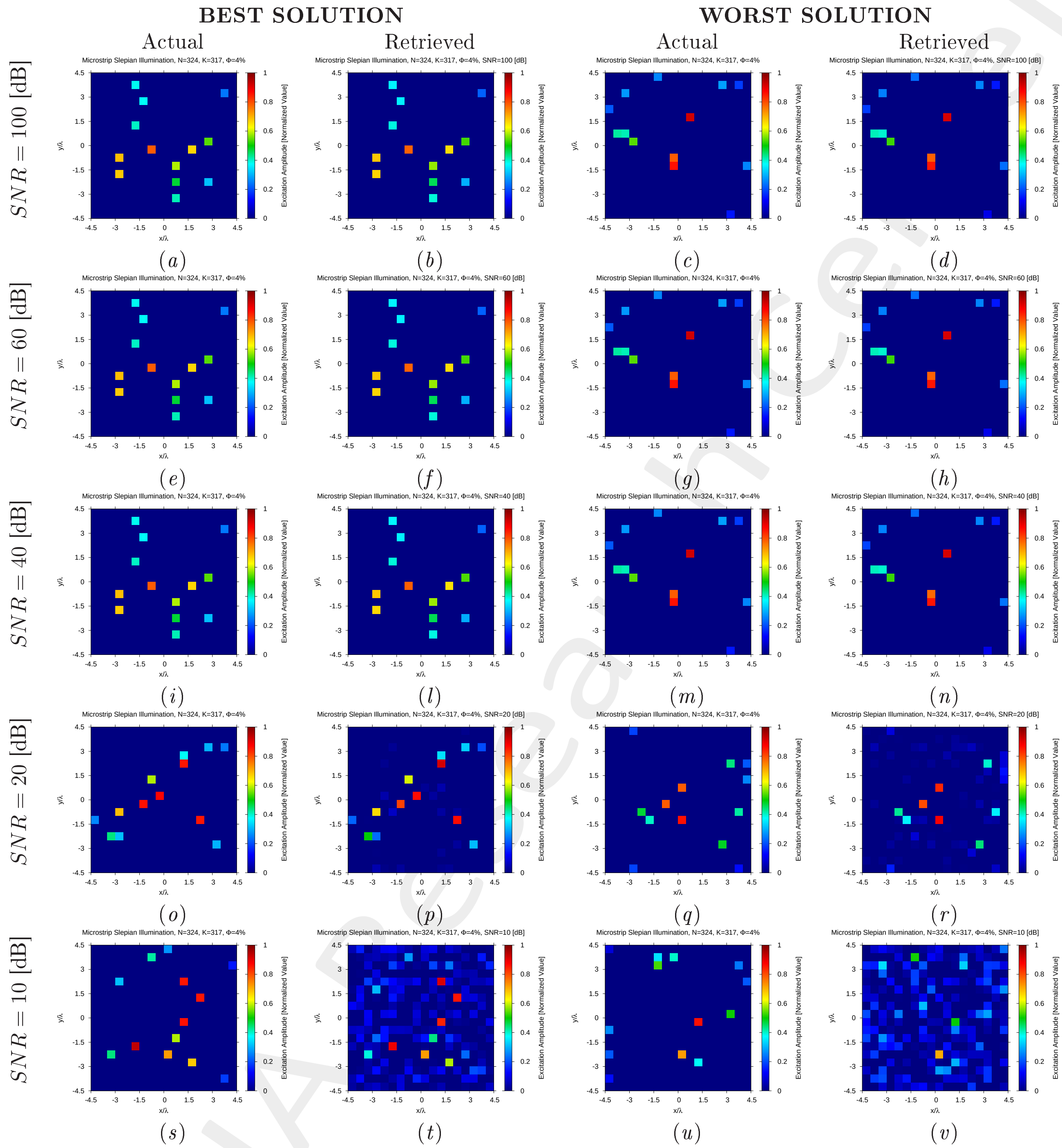

Figure 13: *Microstrip Patches Array* ($N = 324$, $d_x = d_y = 0.5$ [λ], $\Phi = 4\%$) - Best and worst reconstructions under several SNR values.

$\Phi = \frac{N_f}{N} = 8\%$ $(N_f = 26)$ **- Best and Worst** BCS **Reconstructions**

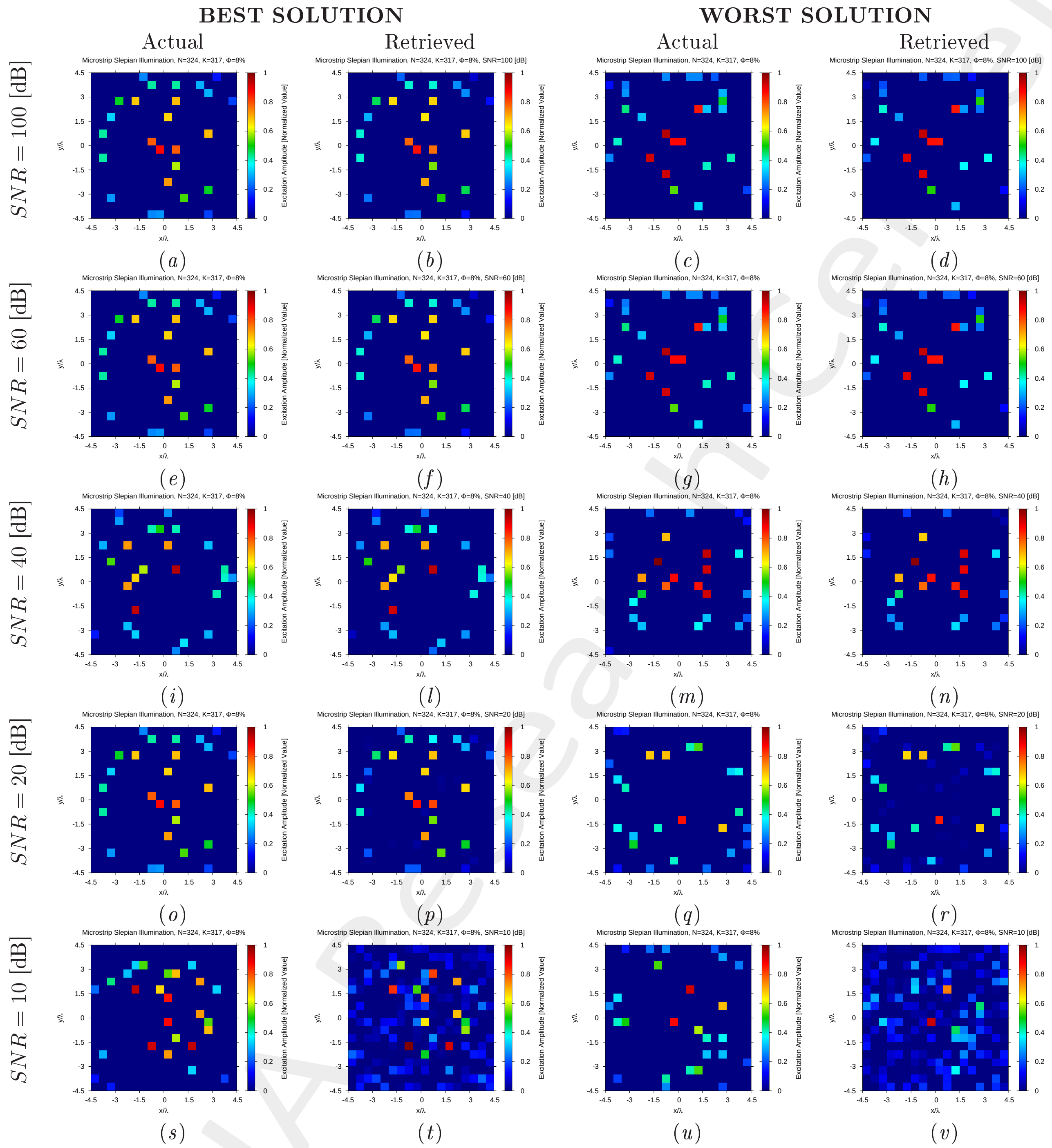

Figure 14: *Microstrip Patches Array* ($N = 324$, $d_x = d_y = 0.5$ $[\lambda]$, $\Phi = 8\%$) - Best and worst reconstructions under several SNR values.

$\Phi = \frac{N_f}{N} = 16\%$ ($N_f = 52$) - **Best and Worst** BCS **Reconstructions**

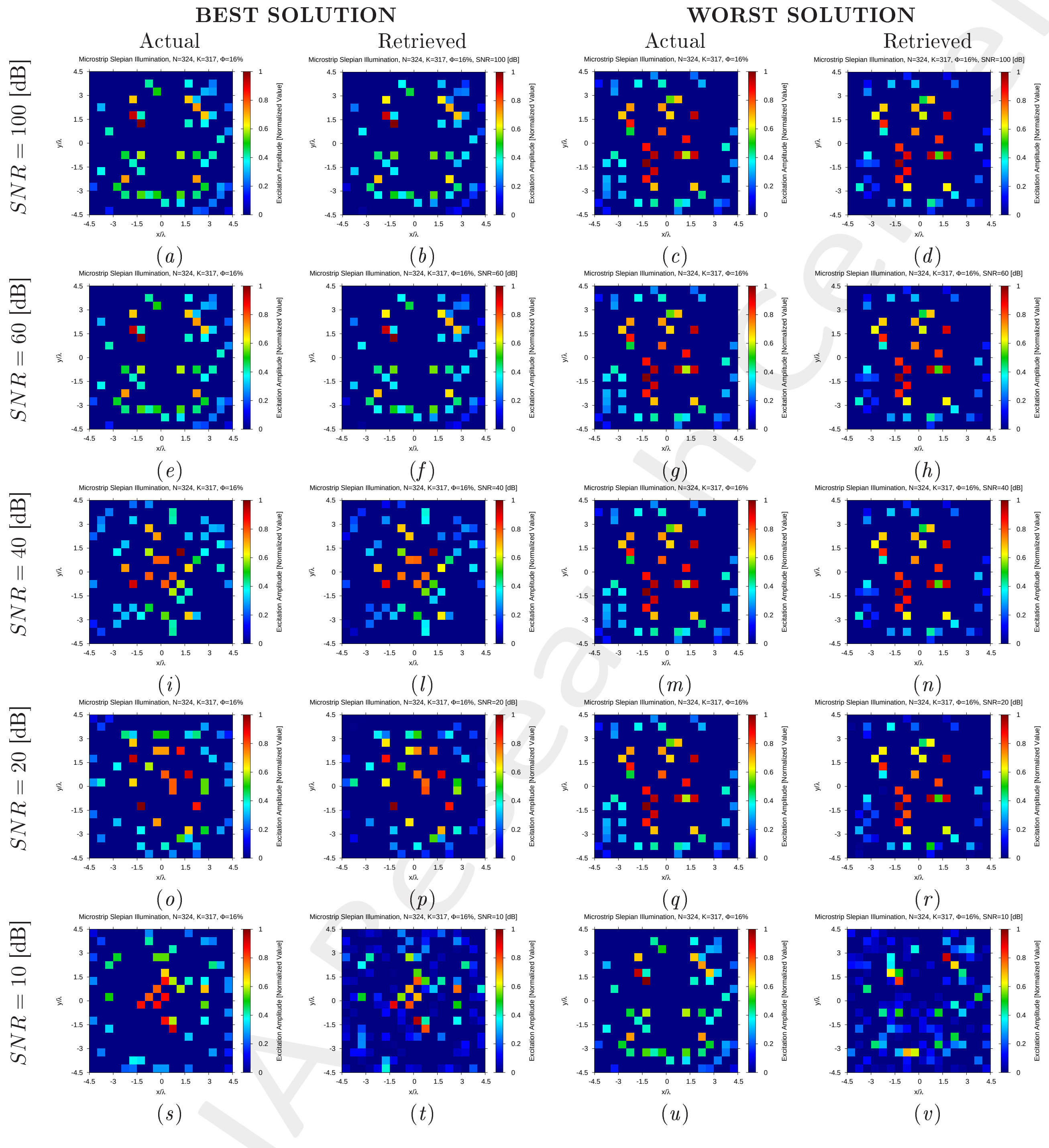

Figure 15: *Microstrip Patches Array* ($N = 324$, $d_x = d_y = 0.5$ $[\lambda]$, $\Phi = 16\%$) - Best and worst reconstructions under several SNR values.

Diagnosis Error and Confidence Level

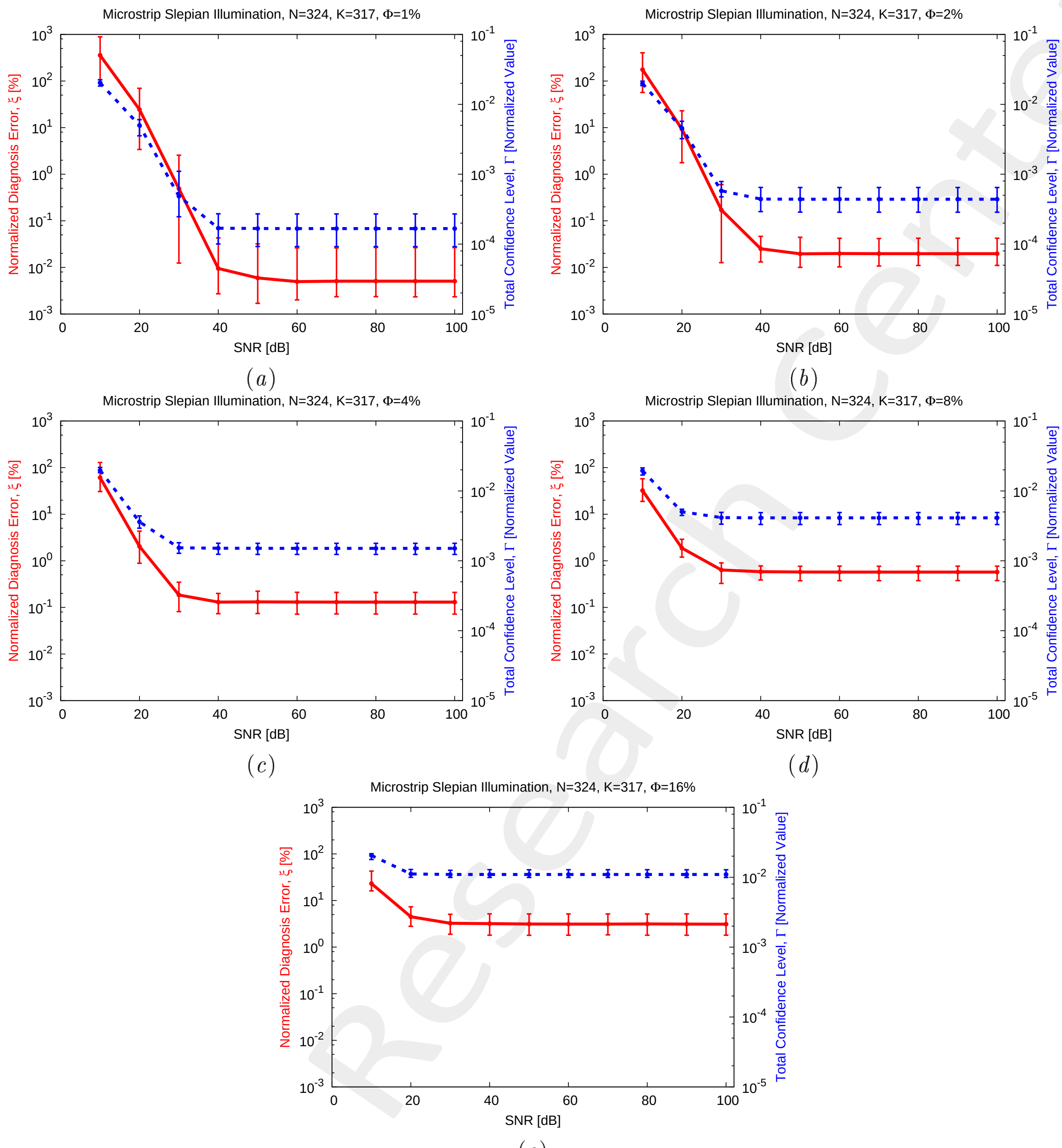

Figure 16: *Microstrip Patches Array* ($N = 324$, $d_x = d_y = 0.5$ $[\lambda]$) - Behavior of the average, minimum and maximum diagnosis error (ξ) and total confidence level (Γ) versus the SNR, for (a) $\Phi = 1\%$, (b) $\Phi = 2\%$, (c) $\Phi = 4\%$, (d) $\Phi = 8\%$, and (e) $\Phi = 16\%$.

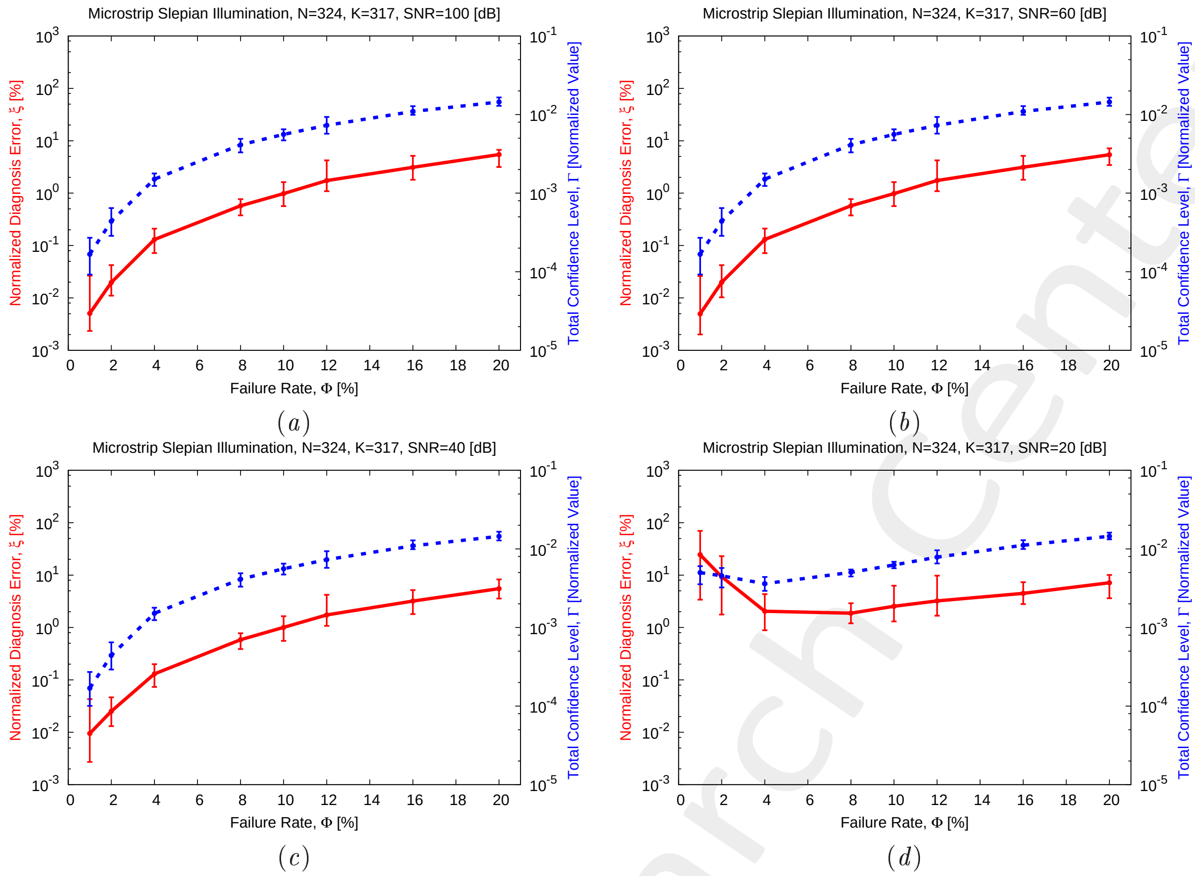

Figure 17: *Microstrip Patches Array* ($N = 324$, $d_x = d_y = 0.5$ [λ]) - Behavior of the average, minimum and maximum diagnosis error (ξ) and total confidence level (Γ) versus the failure rate (Φ), for (a) $SNR = 100$ [dB], (b) $SNR = 60$ [dB], (c) $SNR = 40$ [dB], and (d) $SNR = 20$ [dB].

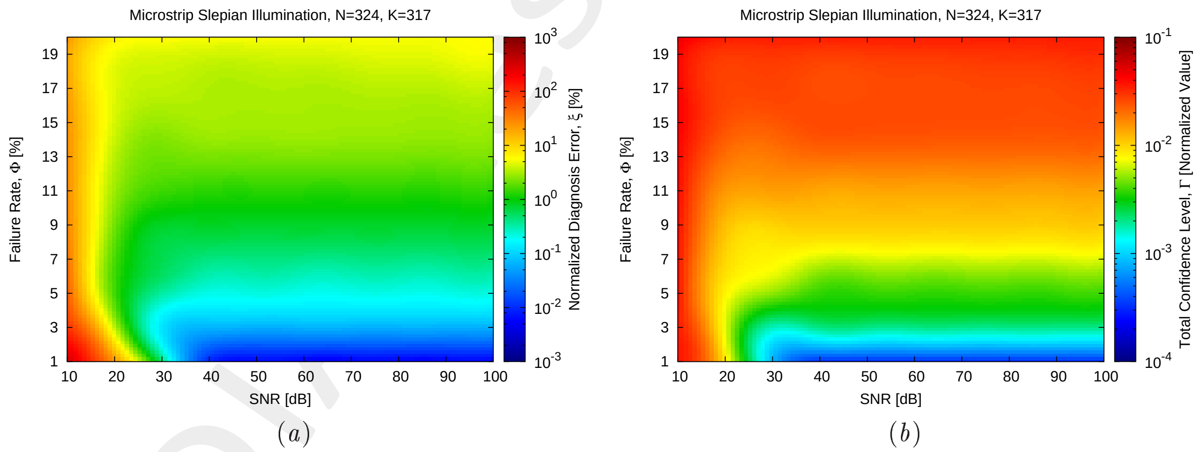

Figure 18: *Microstrip Patches Array* ($N = 324$, $d_x = d_y = 0.5$ [λ]) - Behavior of the average diagnosis error (ξ) and total confidence level (Γ) versus the SNR and the failure rate (Φ).

1.3 Comparison vs Array Size (N)

The following figures summarize the diagnosis outcomes when considering a variation of the number of radiators, N. More precisely, Fig. 19 reports the average diagnosis error and confidence level when considering a failure rate of $\Phi = 4\%$, while results for $\Phi = 16\%$ are shown in Fig. 20.

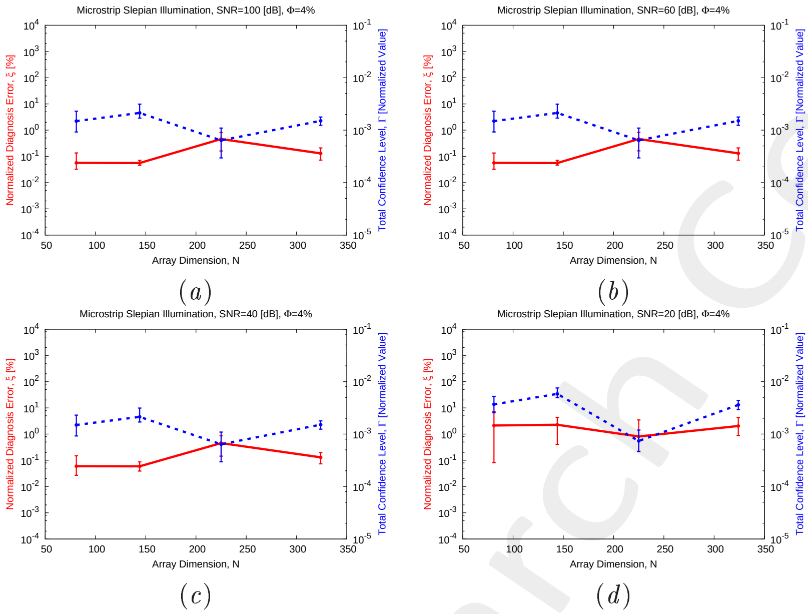

Figure 19: *Microstrip Patches Array* ($N = 324$, $d_x = d_y = 0.5$ [λ], $\Phi = 4\%$) - Behavior of the average, minimum and maximum diagnosis error (ξ) and total confidence level (Γ) versus the array size (N), for (a) $SNR = 100$ [dB], (b) $SNR = 60$ [dB], (c) $SNR = 40$ [dB], and (d) $SNR = 20$ [dB].

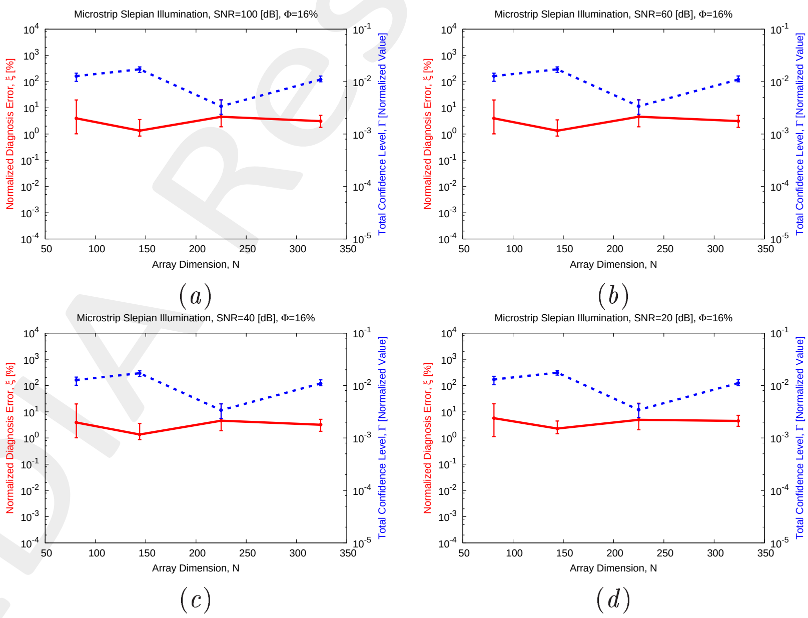

Figure 20: *Microstrip Patches Array* ($N = 324$, $d_x = d_y = 0.5$ [λ], $\Phi = 16\%$) - Behavior of the average, minimum and maximum diagnosis error (ξ) and total confidence level (Γ) versus the array size (N), for (a) $SNR = 100$ [dB], (b) $SNR = 60$ [dB], (c) $SNR = 40$ [dB], and (d) $SNR = 20$ [dB].

More information on the topics of this document can be found in the following list of references.

References

[1] G. Oliveri, L. Poli, and A. Massa "Maximum efficiency beam synthesis of radiating planar arrays for wireless power transmission," *IEEE Trans. Antennas Propag.*, vol. 61, no. 5, pp. 2490-2499, May 2013.

[2] P. Rocca, G. Oliveri, R. J. Mailloux, and A. Massa "Unconventional phased array architectures and design methodologies - A Review," *Proc. IEEE*, vol. 104, no. 3, pp. 544-560, Mar. 2016.

[3] G. Oliveri, G. Gottardi, F. Robol, A. Polo, L. Poli, M. Salucci, M. Chuan, C. Massagrande, P. Vinetti, M. Mattivi, R. Lombardi, and A. Massa "Co-design of unconventional array architectures and antenna elements for 5G base stations," *IEEE Trans. Antennas Propag.*, vol. 65, no. 12, pp. 6752-6767, Dec. 2017.

[4] G. Oliveri, P. Rocca, and A. Massa "Reliable diagnosis of large linear arrays - a Bayesian compressive sensing approach," *IEEE Trans. Antennas Propag.*, vol. 60, no. 10, pp. 4627-4636, Oct. 2012.

[5] M. Salucci, A. Gelmini, G. Oliveri, and A. Massa "Planar arrays diagnosis by means of an advanced Bayesian compressive processing," *IEEE Trans. Antennas Propag.*, vol. 66, no. 11, pp. 5892-5906, Nov. 2018.

[6] A. Massa, P. Rocca, and G. Oliveri "Compressive sensing in electromagnetics - A review," *IEEE Antennas Propag. Mag.*, pp. 224-238, vol. 57, no. 1, Feb. 2015.

[7] G. Oliveri, M. Salucci, N. Anselmi, and A. Massa "Compressive sensing as applied to inverse problems for imaging: theory, applications, current trends, and open challenges," *IEEE Antennas Propag. Mag.*, vol. 59, no. 5, pp. 34-46, Oct. 2017.

[8] P. Rocca, M. A. Hannan, M. Salucci, and A. Massa "Single-snapshot DoA estimation in array antennas with mutual coupling through a multi-scaling Bayesian compressive sensing strategy," *IEEE Trans. Antennas Propag.*, vol. 65, no. 6, pp. 3203-3213, Jun. 2017.

[9] M. Carlin, P. Rocca, G. Oliveri, F. Viani, and A. Massa "Directions-of-arrival estimation through Bayesian Compressive Sensing strategies," *IEEE Trans. Antennas Propag.*, vol. 61, no. 7, pp. 3828-3838, Jul. 2013.

[10] L. Poli, G. Oliveri, P. Rocca, M. Salucci, and A. Massa "Long-distance WPT unconventional arrays synthesis," *J. Electromagn. Waves Appl.*, vol. 31, no. 14, pp. 1399-1420, Jul. 2017.

[11] G. Oliveri, M. Salucci, and A. Massa "Synthesis of modular contiguously clustered linear arrays through a sparseness-regularized solver," *IEEE Trans. Antennas Propag.*, vol. 64, no. 10, pp. 4277-4287, Oct. 2016.

[12] G. Oliveri and A. Massa "Bayesian compressive sampling for pattern synthesis with maximally sparse non-uniform linear arrays," *IEEE Trans. Antennas Propag.*, vol. 59, no. 2, pp. 467-481, Feb. 2011.

[13] N. Anselmi, G. Oliveri, M. A. Hannan, M. Salucci, and A. Massa "Color compressive sensing imaging of arbitrary-shaped scatterers," *IEEE Trans. Microw. Theory Techn.*, vol. 65, no. 6, pp. 1986-1999, Jun. 2017.

[14] N. Anselmi, G. Oliveri, M. Salucci, and A. Massa "Wavelet-based compressive imaging of sparse targets," *IEEE Trans. Antennas Propag.*, vol. 63, no. 11, pp. 4889-4900, Nov. 2015.

[15] L. Poli, G. Oliveri, F. Viani, and A. Massa "MT-BCS-based microwave imaging approach through minimum-norm current expansion," *IEEE Trans. Antennas Propag.*, vol. 61, no. 9, pp. 4722-4732, Sep. 2013.

[16] G. Oliveri, N. Anselmi, and A. Massa "Compressive sensing imaging of non-sparse 2D scatterers by a total-variation approach within the Born approximation," *IEEE Trans. Antennas Propag.*, vol. 62, no. 10, pp. 5157-5170, Oct. 2014.

[17] L. Poli, G. Oliveri, and A. Massa "Imaging sparse metallic cylinders through a local shape function bayesian compressive sensing approach," *J. Opt. Soc. Am. A*, vol. 30, no. 6, pp. 1261-1272, 2013.

[18] L. Poli, G. Oliveri, P. Rocca, and A. Massa "Bayesian compressive sensing approaches for the reconstruction of two-dimensional sparse scatterers under TE illumination," *IEEE Trans. Geosci. Remote Sens.*, vol. 51, no. 5, pp. 2920-2936, May 2013.

[19] L. Poli, G. Oliveri, and A. Massa "Microwave imaging within the first-order Born approximation by means of the contrast-field Bayesian compressive sensing," *IEEE Trans. Antennas Propag.*, vol. 60, no. 6, pp. 2865-2879, Jun. 2012.

[20] G. Oliveri, L. Poli, P. Rocca, and A. Massa "Bayesian compressive optical imaging within the Rytov approximation," *Opt. Lett.*, vol. 37, no. 10, pp. 1760-1762, 2012.

[21] G. Oliveri, P. Rocca, and A. Massa "A Bayesian compressive sampling-based inversion for imaging sparse scatterers," *IEEE Trans. Geosci. Remote Sens.*, vol. 49, no. 10, pp. 3993-4006, Oct. 2011.

[22] N. Anselmi, L. Poli, G. Oliveri, and A. Massa "Iterative multi-resolution bayesian CS for microwave imaging," *IEEE Trans. Antennas Propag.*, vol. 66, no. 7, pp. 3665-3677, Jul. 2018.

[23] L. Poli, P. Rocca, G. Oliveri, and A. Massa "Failure correction in time-modulated linear arrays," *IET Radar, Sonar & Navigation*, vol. 8, no. 3, pp. 195-201, 2014.